AFRL-RX-WP-TP-2010-4070

SMALL FATIGUE CRACK GROWTH AND FAILURE MODE TRANSITIONS IN A Ni-BASE SUPERALLOY AT ELEVATED TEMPERATURE (Preprint)

M. J. Catona

Behavior/Life Prediction Section
Metals Branch

S. K. Jha

Universal Technology Corporation

FEBRUARY 2010
Interim Report

AIR FORCE RESEARCH LABORATORY
MATERIALS AND MANUFACTURING DIRECTORATE
WRIGHT-PATTERSON AIR FORCE BASE, OH 45433-7750
AIR FORCE MATERIEL COMMAND
UNITED STATES AIR FORCE

REPORT DOCUMENTATION PAGE

Form Approved
OMB No. 0704-0188

1. REPORT DATE *(DD-MM-YY)*	2. REPORT TYPE	3. DATES COVERED *(From - To)*
February 2010	Journal Article Preprint	01 February 2010 – 01 February 2010

4. TITLE AND SUBTITLE
SMALL FATIGUE CRACK GROWTH AND FAILURE MODE TRANSITIONS IN A Ni-BASE SUPERALLOY AT ELEVATED TEMPERATURE (Preprint)

5a. CONTRACT NUMBER
IN HOUSE

5b. GRANT NUMBER

5c. PROGRAM ELEMENT NUMBER
62102F

6. AUTHOR(S)
M. J. Catona (Metals Branch, Behavior/Life Prediction Section (AFRL/RXLMN))
S. K. Jha (Universal Technology Corporation)

5d. PROJECT NUMBER
4347

5e. TASK NUMBER
RG

5f. WORK UNIT NUMBER
M02R3000

7. PERFORMING ORGANIZATION NAME(S) AND ADDRESS(ES)

Behavior/Life Prediction Section (AFRL/RXLMN)
Metals Branch , Metals, Ceramics, and Nondestructive Evaluation Division
Materials and Manufacturing Directorate, Air Force Research Laboratory
Wright-Patterson Air Force Base, OH 45433-7750
Air Force Materiel Command, United States Air Force

Universal Technology Corporation

8. PERFORMING ORGANIZATION REPORT NUMBER
AFRL-RX-WP-TP-2010-4070

9. SPONSORING/MONITORING AGENCY NAME(S) AND ADDRESS(ES)
Air Force Research Laboratory
Materials and Manufacturing Directorate
Wright-Patterson Air Force Base, OH 45433-7750
Air Force Materiel Command
United States Air Force

10. SPONSORING/MONITORING AGENCY ACRONYM(S)
AFRL/RXLMN

11. SPONSORING/MONITORING AGENCY REPORT NUMBER(S)
AFRL-RX-WP-TP-2010-4070

12. DISTRIBUTION/AVAILABILITY STATEMENT
Approved for public release; distribution unlimited.

13. SUPPLEMENTARY NOTES
PAO case number 88 ABW-2009-5233, cleared 21 December 2009. This work was funded in whole or in part by Department of the Air Force work unit M02R3000. The U.S. Government has for itself and others acting on its behalf an unlimited, paid-up, nonexclusive, irrevocable worldwide license to use, modify, reproduce, release, perform, display, or disclose the work by or on behalf of the U. S. Government. Submitted to the International Journal of Fatigue. Paper contains color.

14. ABSTRACT
A study of the long and small fatigue crack growth behavior in IN100 tested at 650 °C both with and without dwell periods is summarized. A significant small crack effect is evident in this alloy, and it is observed that the influence of loading variables on small crack behavior is profoundly different from that on long cracks. While a 6-second dwell has negligible effect on long crack growth rates, it results in more than an order of magnitude faster growth for small cracks (~30 m to 1mm). Long crack growth is dominated by intergranular cracking both with and without 6-sec dwell. Small crack growth mode depends on numerous factors including crack size, dwell time, exposure to environment, and character of initiation site. Transitions in small crack growth modes and the operative crack growth mechanisms are discussed.

15. SUBJECT TERMS
Fatigue, Small crack, Fractography, Intergranular, Transgranular, Dwell

16. SECURITY CLASSIFICATION OF:			17. LIMITATION OF ABSTRACT:	18. NUMBER OF PAGES	19a. NAME OF RESPONSIBLE PERSON (Monitor)
a. REPORT	b. ABSTRACT	c. THIS PAGE			Reji John
Unclassified	Unclassified	Unclassified	SAR	34	19b. TELEPHONE NUMBER *(Include Area Code)* N/A

Standard Form 298 (Rev. 8-98)
Prescribed by ANSI Std. Z39-18

Small Fatigue Crack Growth and Failure Mode Transitions in a Ni-Base Superalloy at Elevated Temperature

M. J. Caton[a*] and S. K. Jha[b]

[a] *Materials and Manufacturing Directorate, Air Force Research Laboratory (AFRL/RXLMN), Wright-Patterson AFB, OH 45433-7817, USA*

[b] *Universal Technology Corporation, 1270 N. Fairfield Road, Dayton, OH 45432, USA*

Abstract

A study of the long and small fatigue crack growth behavior in IN100 tested at 650°C both with and without dwell periods is summarized. A significant small crack effect is evident in this alloy, and it is observed that the influence of loading variables on small crack behavior is profoundly different from that on long cracks. While a 6 second dwell has negligible effect on long crack growth rates, it results in more than an order of magnitude faster growth for small cracks (~30 μm to 1mm). Long crack growth is dominated by intergranular cracking both with and without 6 sec dwell. Small crack growth mode depends on numerous factors including crack size, dwell time, exposure to environment, and character of initiation site. Transitions in small crack growth modes and the operative crack growth mechanisms are discussed.

Keywords: Fatigue; Small crack; Fractography; Intergranular; Transgranular; Dwell

1. Introduction

The current life-management approaches for fracture-critical components in military turbine engines are based on the expected worst-case behavior, where safe life limits are determined from a 1 in 1,000 probability of the existence of a crack of detectable size (typically ~ 800 μm). These life limits are traditionally established empirically by extrapolating random deviations from the mean lifetime [1]. However, recent studies of turbine engine alloys have shown that the life-limiting behavior is often not accurately predicted by applying random deviations about the mean life, since the worst-case and mean lifetime distributions can frequently result from distinctly different failure mechanisms [2-4]. Therefore, a more accurate prediction of life-limiting behavior is sought through mechanistically-derived probabilistic methods.

Fig. 1 shows an example of fatigue lifetimes previously reported [2] for IN100, a common powder metallurgy (P/M) Ni-base superalloy used in turbine engines. Here it is seen that the trend in the mean lifetime, shown by the dashed lines, is very different from that observed for minimum life specimens. Further, the hatched regions, which indicate the range of predicted life assuming immediate crack initiation, show good agreement with the worst-case failures. This strongly suggests that while the mean life is composed primarily of crack initiation, the minimum life distributions are dominated by crack growth, where the cycles required to initiate a crack can be considered negligible. Improved accuracy of predicted worst-case life limits can therefore be achieved by characterizing crack growth behavior.

To ensure the accuracy of crack growth-based predictions, it is important to identify the degree to which small crack effects are present under relevant loading conditions. Fig. 2 shows the previously reported [2] crack growth behavior for IN100, under both dwell and no dwell loading conditions. It is seen that a significant small crack effect is present in this alloy under these conditions. In addition, these data indicate that the effect of modest changes in loading condition (in this case, the application of 6 second dwell time at peak load) can be profoundly different on small crack growth compared to long crack growth behavior. Aside from a slightly higher crack growth threshold seen with 6 second dwell, the long crack data indicate essentially no effect of the dwell time on growth rates. The small crack data in Fig. 2, on the other hand, show a very significant effect of dwell, where growth rates under the dwell condition can be more than an order of magnitude faster for initial crack growth (crack sizes ~ 50 to 250 μm). The crack growth (CG) life predictions in Fig. 1 include this observed small crack behavior [2].

It is recognized that understanding the early crack growth behavior is critical for developing more accurate, mechanistically-based models of fatigue life limits, thereby enabling safer and more affordable life management practices. This paper provides a detailed examination of small crack growth behavior in IN100, and the mechanisms that drive the worst-case failures under the loading conditions depicted in Fig. 1.

2. Material and experimental procedures

The material examined in this paper is a powder-metallurgy (P/M) processed and subsolvus-treated nickel-base superalloy, IN100, which was reported on previously [4]. The microstructure of the alloy consisted of γ-phase grains and primary, secondary, and tertiary γ' precipitates. The average γ grain size was about 3 - 4 μm and the grain structure was quite equiaxed. In addition to the γ and γ' phases, the microstructure also contained non-metallic particles (NMP) and pores, which are typically contained in powder processed superalloy materials [5, 6]. Note that at least two kinds of NMP were observed, distinguishable by their morphology. One possessed a blocky appearance while the other had a granular, sponge-like morphology. Characteristics of these types of NMP in superalloys have been reported in other studies [5, 6]. From the fatigue failure perspective, however, both types were found to be important and, in the given number of experiments, appeared to produce similar crack initiation sizes and range in lifetimes. Throughout the paper, these are referred to generically as NMPs. In general, the NMPs are somewhat larger than the pores, with equivalent diameters of about 20 to 40 μm, and significantly less prevalent. For more details on the size distributions and volume fractions of the pores and NMP in this alloy, the reader is referred to [4].

The 0.2% yield strength and the ultimate tensile strength of the material at the test temperature of 650°C were about 1100 and 1379 MPa, respectively. The percent elongation at 650°C was about 20% and the elastic modulus was about 186 GPa.

The specimens tested in this study were extracted in the circumferential orientation from a pancake forging of the material. A cylindrical, button-head test specimen with a gage length of 15.2 mm and a diameter of 5 mm was used, as described in [7]. The specimens had a low-stress-ground (LSG) finish. The fatigue tests were conducted using an MTS servo-hydraulic test system with a 646 controller. An electric resistance furnace was mounted on the test frame. A high-temperature button-head gripping assembly was used in conjunction with a standard collet-grip system to transfer load to the sample. The hydraulic grip units were water-cooled.

Temperature-control thermocouples were welded outside of the specimen gage section to maintain the test temperature at the specimen. The tests were performed in load control at a frequency of 0.33 Hz, a stress ratio (R) of 0.05, and a temperature of 650ºC. The effect of dwell was examined, whereby a series of specimens were tested with a 6 second hold time applied at the peak load. The fracture surfaces of all specimens were examined using scanning electron microscopy to identify and characterize crack initiation sites and crack growth morphology.

Small crack growth rates were monitored for numerous fatigue specimens using a standard replication technique. The gage sections of the small crack specimens were electropolished, typically removing about 10 to 15 μm of material, and achieving a mirror finish, which facilitated the observation of cracks on the acetate replication tape. The small crack growth tests were periodically interrupted, the specimen was cooled to room temperature, and a replication of the entire surface of the gage section was taken while the specimen was held under a static tensile load of ~70% σ_{max}. Small crack growth rates were calculated using a 3-point sliding polynomial fit to the crack size versus cycle data. The stress intensity factor range, ΔK, was calculated using a solution from Raju and Newman [9] for a surface crack in a rod and assuming a semi-circular crack shape (i.e., depth/half length = a/c = 1), and the reported data represents ΔK at the surface tip (i.e., $\phi = 0°$).

Long fatigue crack growth rates were acquired using two different sizes of compact tension, C(T), specimens with nominal height, width, and thickness of 24 mm, 20 mm, and 5 mm, respectively, or 48 mm, 40 mm, and 10 mm, respectively. No difference in crack growth rates was observed between these two C(T) specimen sizes. Long crack tests were conducted at 650 ºC, a stress ratio (R) of 0.05, and using a triangle waveform at a frequency of 0.33 Hz, both with and without a 6 second dwell period applied at the peak load. A single threshold test was conducted for both the 6 second dwell and no dwell loading conditions, following the standard K-decreasing procedure outlined in ASTME647, where crack size was monitored using direct current potential difference (DCPD) measurements. Additional data were acquired at discrete ΔK levels within the Paris regime of the crack growth curves (ΔK ranging from 14.25 to 57 MPa-$m^{1/2}$) using a K_{max}-constant technique to enable the acquisition of a significant amount of data within relatively short times and from relatively few specimens. In this procedure, blocks of constant loading condition are applied for a crack extension adequate to give a steady state growth rate. In this case, individual blocks resulted in approximately 0.3 mm of crack extension. The maximum K levels were always maintained constant or increased from one block of loading to the next to minimize load interaction effects. Data from K_{max}-constant loading were acquired from eight separate specimens.

3. Results and discussion

3.1 Comparing Long and Small Crack Growth Behavior

Fig. 2 compares the previously reported long and small crack growth rates observed in this alloy under loading both with and without a 6 second dwell applied at the peak load [2]. The long crack data were acquired from C(T) specimens, where the crack lengths ranged from about 5 to 30 mm with through-thicknesses of 5 or 10 mm. A single threshold test is represented for both loading conditions, and data from eight separate specimens are represented in the Paris regime for discrete ΔK levels ranging from 14.25 to 57.0 MPa-$m^{1/2}$. It is seen that there is very

little scatter in the long crack data for both loading conditions. Both data sets show a scatter of about 1.5X in the Paris regime. Additionally, Fig. 2 demonstrates that a 6 second dwell period has a negligible effect on long crack growth rate, with the exception of a slightly higher crack growth threshold observed under 6 second dwell. The long crack threshold was determined to be 12.3 MPa-$m^{1/2}$ under loading with no dwell and 13.6 MPa-$m^{1/2}$ under 6 second dwell loading. These observations are consistent with other reports in the literature. Lynch et al. [10, 11] reported higher threshold in Waspaloy and Alloy 718 under 60 second dwell at peak load than with no hold time. At higher ΔK, however, faster growth rates were observed under dwell. This behavior was shown to be temperature dependent, in that at lower temperatures, dwell time had minimal influence on crack growth rate. The authors also reported insignificant effect of 2 and 10 second dwell times on long crack growth rates [10]. It has been proposed that higher thresholds under dwell conditions could result from enhanced oxidation-induced crack closure (OICC) and roughness-induced crack closure (RICC), as well as reduction in driving force due to crack branching along grain boundaries. These factors can be considered as being driven by the environmental exposure. At higher ΔK levels, the increased contribution of creep crack growth and lack of crack closure effects is thought to promote faster growth rates [10, 11]. Note, that the Waspaloy used in the above studies had the γ grain size of 70-100 μm and the Alloy 718 was reported to predominantly contain 2-10 μm recrystallized grains and some unrecrystallized grains, 20 μm x 50 μm in size. In contrast, the IN100 alloy in the present study had equiaxed grains of about 3 – 4 μm size. Sadananda and Shahinian [12] attributed the slower crack growth rates with increasing dwell time at lower ΔK to the creep crack growth threshold. Their study was conducted on Udimet 700 with a grain size of about 100 μm. A creep-assisted crack-tip stress relaxation mechanism was suggested as being dominant below the threshold for creep crack growth, promoting slower growth rates. Clearly, a combination of these mechanisms can possibly be operational in any given case, where the degree of contribution of a factor may depend on the grain size, temperature, and loading regime. Given the small grain size in the present study, the environmentally-induced mechanisms could play a stronger role via preferential oxidation at grain boundaries and the associated branching of the crack.

The mechanism of dwell-time effect on the long crack behavior, which has been the focus of several studies, is important in physics-based prediction of lifetime limits, but equally imperative is an accurate representation of the small crack growth regime under dwell conditions. It is clear from Fig. 2 that there is a significant small crack effect present in this alloy under both dwell and no-dwell loading conditions. That is, the small cracks are observed to grow at ΔK levels less than the long crack thresholds and at faster rates than long cracks for a given ΔK. Perhaps most noteworthy from Fig. 2, is the profound influence of 6 second dwell on small crack growth rates. While this modest hold time has essentially no effect on long crack growth rates, the 6 second dwell results in significantly faster growth rates when the cracks are small (~30 μm to ~1.2 mm), where the difference can be well over an order of magnitude at low ΔK levels. In addition, for ΔK levels less than about 10 MPa-$m^{1/2}$ there is significantly more scatter observed in the small crack growth behavior under loading with no dwell. The large scatter seen in the small cracks at these sizes (~30 to 100 μm) is thought to be largely due to the influence of local microstructure. The crack front will temporarily arrest at hard barriers, such as grains oriented unfavorably for slip, before advancing rapidly to the next barrier. These “starts and stops” are not observed under the 6 second dwell loading. The 6 second dwell period introduces time-dependent mechanisms, particularly creep and environmentally-assisted embrittlement of grain boundaries,

which enable the crack front to overcome the barriers that would otherwise cause temporary deceleration or arrest without the dwell period.

The fracture surfaces for both long and small cracks shown in Fig. 3 provide some insight into the crack growth modes operative in the different regimes. Figs. 3 (a) and (b) show SEM photos of the fracture surfaces of long crack specimens tested under no dwell and 6 second dwell, respectively. Both of these images were taken in a region of near-threshold crack growth, where the ΔK level was 14.25 MPa-$m^{1/2}$ and crack length was ~10 mm. Under both dwell and no dwell conditions, long crack growth is seen to be dominated by intergranular crack growth. While the preferred path for long crack growth is along grain boundaries under both dwell and no dwell loading, the three dimensional structure of the grains appears more clearly defined in Fig. 3 (b), likely resulting from enhanced cavitation and oxidation at grain boundaries during the 6 second dwell.

Figs. 3 (c) and (d) show SEM images for the fracture surfaces of small fatigue cracks grown under no dwell and 6 second dwell loading, respectively. Both of these cracks were tested with σ_{max} = 1,150 MPa. It is observed in Fig. 3 (d) that under 6 second dwell loading, the crack growth mode is fully intergranular from the earliest sizes. Fig 3 (c), on the other hand, illustrates that the early crack growth under loading with no dwell is composed of a mixture of both intergranular and transgranular growth. Fig. 4 provides a lower magnification image of the same crack from Fig. 3 (c), showing how the crack growth mode evolves as the crack grows. Significant regions of transgranular growth are observed for crack sizes less than a depth of about 135 μm and surface length of about 220 μm. Beyond this size, the crack growth mode is observed to be fully intergranular and resembles the morphology seen in long crack specimens. Pang and Reed [8] reported a very similar transgranular to intergranular mode shift for small crack growth in a U720Li alloy with similar grain size. Fig. 4 also shows the estimated ΔK levels for various crack depths, using the solution from Raju and Newman [9] for a surface crack in a rod and assuming a semi-circular crack shape (i.e., depth/half length = a/c = 1). The size at which this transition to fully intergranular crack growth occurs under this loading condition (650°C, 0.33 Hz, R = 0.05, σ_{max} = 1,150 MPa, No Dwell) is seen to be quite consistent from specimen to specimen. Numerous specimens were examined and the transition is observed to occur at crack depths ranging from ~110 to 150 μm and full crack lengths, 2c, ranging from ~210 to 250 μm. This corresponds to ΔK levels of about 13 to 16 MPa-$m^{1/2}$, which is slightly greater than the long crack threshold. The repeatable nature of the crack size at which this transition in crack growth mode occurs suggests that it is controlled largely by a mechanical driving force. It is possible that the plastic zone size ahead of the crack tip or the crack tip opening displacement (CTOD) develop to a critical level at this transition point such that the environmental attack of grain boundaries becomes the exclusive mode of crack growth.

3.2 Key Factors Controlling Small Crack Growth

3.2.1 Role of Environment on Crack Growth Mode

The environment plays a critical role in determining both crack growth mode and the rate of growth in superalloys at elevated temperature. A number of studies have reported the general observation of reduced fatigue crack growth rates and a shift from intergranular to transgranular crack growth in vacuum when compared to testing in air [13 - 18]. Both Hide et al. [13] and

Onofrio et al. [14] show a slower crack growth rate and a shift from transgranular growth in vacuum to intergranular growth in air for U720 Li. Similar observations were also reported by Gayda and Miner [15] for Astroloy, where the prevalence of intergranular fracture morphology in air was shown to be dependent on grain size. With only a few exceptions (e.g., [14] and [17]), most studies of environmental effect on fatigue crack growth have been focused on the long-crack regime. It is not clear to what extent, if at all, the mechanisms of the environmental effect on long crack behavior can be applied to the small crack regime. However, the data in Fig. 2 showing an appreciably different sensitivity to hold time between long and small cracks suggest that a thorough understanding of the mechanisms controlling small crack growth is critical to achieve accurate predictions of life-limiting behavior and cannot be adequately characterized from long crack data. Fractographic examination of specimens tested in the current study can begin to illuminate the environmental influence on small crack growth under the given loading conditions.

Fig. 5 shows the fracture surface of a specimen tested without dwell that failed from an internally initiated fatigue crack. The crack emanating from the subsurface NMP is seen to have grown quite symmetrically and broke the specimen surface at a crack size of about 575 μm. Prior to breaking the surface, the crack growth occurred in a pseudo-vacuum. Fig. 5 (b) provides a higher magnification image of the point at which the crack front is first exposed to the environment. It can be seen that a dramatic shift in crack growth morphology occurs as a result of the presence of the air environment. The internal crack growth under pseudo-vacuum conditions is seen to be quite transgranular in nature (left side of Fig 5 (b)). However, once the crack front is exposed to air, the fractography indicates an immediate shift to fully intergranular crack growth mode (right side of Fig 5 (b)). The stress intensity factor for the crack size where this transition occurs (a ~ 575 μm) can be estimated using a solution from Newman and Raju [19] for an embedded crack in a finite plate and is calculated to be ~31 MPa-$m^{1/2}$. It was found that a similar ΔK solution from Benthem and Koiter [20] for an embedded crack in a cylindrical rod (also found in [21]) provided essentially identical results. This level of ΔK is significantly greater than the long crack threshold for no dwell loading of ~12.3 MPa-$m^{1/2}$. It is also significantly greater than the level at which a repeatable transition to fully intergranular growth is observed for small cracks exposed to air (~13 to 16 MPa-$m^{1/2}$) as illustrated in Fig. 4.

Fig. 6 shows the fracture surface of a specimen tested with 6 second dwell loading that failed from an internally initiated crack. Similar to Fig. 5, this crack grew quite symmetrically from the NMP initiation site, and broke the surface of the specimen at a size of about 370 μm. The specimen in Fig. 6 was tested at σ_{max} = 1,000 MPa, giving an estimated ΔK of 21.4 MPa-$m^{1/2}$ for the size where the crack front is first exposed to the environment. This ΔK level is somewhat lower than that of the transition crack size in Fig. 5, but still appreciably greater than the long crack threshold for 6 second dwell loading (13.6 MPa-$m^{1/2}$). Like the case for no dwell loading in Fig. 5, a very distinct transition in crack growth mode is seen in Fig. 6. Once the crack is exposed to the air environment, crack growth becomes fully intergranular. While the internal crack growth under pseudo-vacuum conditions is seen to be transgranular in nature (left side of Fig 6 (b)), there is more evidence of creep cavitation than was seen in the internal crack growth with no dwell.

The dramatic shift in crack growth morphology in Figs. 5 and 6 provides strong evidence that the mode of intergranular fatigue crack growth in this alloy under the given loading conditions requires exposure to the environment. The dominant mechanism responsible for the observed intergranular crack growth is likely environmentally-assisted embrittlement of grain boundaries

leading to brittle fracture. The time-dependent, diffusion-controlled contribution to the crack growth in superalloys has been studied by several researchers who examined sustained-load crack growth at elevated temperatures. Carpenter et al. [22] examined crack growth in IN718 at temperatures greater than 500°C and described the SAGBO (stress-assisted grain boundary oxidation) mechanism, emphasizing the importance of Nb-oxide layer formation at the grain boundaries leading to brittle intergranular fracture. Krupp et al. [23] studied the effect of environment on crack growth in IN718 under load-relaxation testing at 650°C, and proposed a more general mechanism of "dynamic embrittlement," whereby an embrittling species from the surrounding environment can diffuse into grain boundaries exposed to high tensile stress leading to brittle decohesion along the grain boundary. Huang et al. [24] more closely examined the role of Nb on sustained-load crack growth at temperatures between 600°C and 700°C in an alloy similar to IN100, concluding that the presence of Nb-rich carbides do in fact enhance crack growth in oxygen (>4 orders of magnitude faster growth in oxygen than in argon). However, a Nb-free composition of this alloy also showed significant susceptibility to enhanced crack growth with ~3 orders of magnitude faster intergranular growth in oxygen than the transgranular growth observed in argon. In addition, Huang et al. cite a wide variation in crack growth rates for different Nb-free alloys (including IN100), suggesting that different mechanisms for oxygen-enhanced crack growth will be operative in Ni-base superalloys of different composition and microstructure.

Besides increasing the creep contribution to crack growth rate, an application of dwell time under lab-air conditions also enhances the environmental contribution. As discussed previously with reference to Figs. 3 (c and d), clear differences in fracture modes during early small crack growth with and without a dwell period further illustrate the role of environment in promoting an intergranular crack path. These differences in fracture morphology appear coincident with the significantly faster small-crack growth rates under dwell loading.

3.2.2 Role of Local Microstructure

Naturally-initiated, small surface cracks were monitored using a standard replication technique. Fig. 7 shows the full surface crack length (2c) as a function of cycles for cracks grown in five separate specimens, tested under equivalent no-dwell loading conditions (650°C, 0.33 Hz, R = 0.05, σ_{max} = 1,150 MPa). It is seen that the number of cycles applied before the crack size reaches about 100 μm can vary significantly, ranging from ~1,600 to 17,500 cycles for the five cracks shown in Fig. 7. However, once a crack is beyond this size, the growth behavior is quite similar among all cracks. This significant variability in early crack growth behavior is also depicted in Fig. 2, where the scatter for the no-dwell condition is seen to be very large at low ΔK levels, and then diminishes significantly for ΔK greater than about 10 MPa-$m^{1/2}$. In this regime, cracks are often characterized as microstructurally-small, where the local microstructure exerts significant control over the crack growth behavior. As discussed previously, the large scatter results from the crack front growing rapidly through favorable regions of microstructure and then decelerating or temporarily arresting at local barriers to growth, such as grains oriented unfavorably for slip or perhaps grain boundaries with special character that permit less diffusion of embrittling species [25]. Cracks have been classically designated as *microstructurally*-small for sizes up to about 10 times that of the grain size [26, 27]. However, in the fine grain alloy investigated in the current study, we observed significant fluctuations in small crack growth rate

for crack sizes on the order of 100 μm, which is about 20 to 30 times the grain size. It is recognized that the designation of this critical crack size in relation to a relevant microstructural size scale is somewhat arbitrary. For the purposes of this paper, we are referring to the microstructurally-small crack regime as the size below which significant fluctuations in growth rate are observed. The transition point, where this regime of high variability in small crack growth behavior is surpassed, and the factors controlling it are of interest for better predicting life-limiting fatigue failure mechanisms. Figs. 8 and 9 take a closer look at this transition for two of the surface cracks depicted in Fig. 7, which initiated from pores.

Fig. 8 provides an overview of the crack progression for the pore-initiated crack grown in Specimen A from Fig. 7. Figs. 8 (a) and (b) show the crack growth data, while Fig. 8 (c) shows the fracture surface and images of two replicas indicating surface crack length at 8,000 and 9,500 cycles. It is seen in Fig. 8 (a) that the crack grew relatively slowly up to a size of 93 μm and then temporarily arrested. When reducing this data with a 3-point sliding polynomial curve fit, the crack growth rate is seen in Fig. 8 (b) to fluctuate between 10^{-6} and 10^{-5} mm/cycle. Once the surface crack length surpasses 93 μm, it is seen to grow continuously without detectable deceleration or arrest. It should be noted that the point at which this transition will be identified from the crack growth data is a function of how often crack length measurements are taken. In this case, replicas were taken every 500 cycles. High magnification fractography in the early crack growth regime revealed a somewhat rougher surface layer than is seen in the remainder of the fracture surface. It is thought that this could be an indication of more oxidation products on the fracture surface in this region since it was exposed to the environment for significantly more cycles (~10,000) than the remainder of the fracture surface where the crack grew relatively rapidly (~2,000 cycles). The dashed white outline on the fracture surface in Fig. 8 (c) indicates the region where this enhanced roughness is observed, and provides an estimate of the interior crack front at 8,000 cycles. It is seen that this outlined region corresponds very well with the surface crack length of 93 μm seen in the top replica, where the final period of temporary crack arrest was observed.

Fig. 9 provides an overview of the crack progression for the pore-initiated crack grown in Specimen D from Fig. 7. It should be noted that the crack in Specimen D was not included in the previously published data [2] shown in Fig. 2. It is seen from Fig. 9 (a), that this crack is temporarily arrested for a significant period at a surface length of 90 μm. Beyond this size, the crack grew fairly steadily and then decelerated significantly at a crack length of about 128 μm. Once the crack surpassed the length of 128 μm, it was observed to grow continuously without detectable deceleration or arrest. Like the crack outlined in Fig. 8 for Specimen A, replicas were taken every 500 cycles for Specimen D. The dashed white outline on the fracture surface in Fig. 9 (c) depicts the region where high magnification fractography revealed enhanced surface roughness. Similar to Fig. 8 (c), it is seen that this outlined region corresponds very well with the surface crack length where the final period of temporary crack arrest was observed, in this case depicted in the middle replica for 128 μm. Again, it is thought that the enhanced surface roughness in this region could indicate more oxidation products resulting from longer exposure times to the environment (~23,000 cycles) than for the remainder of the fracture surface, where crack growth was more rapid (~2,000 cycles).

It is interesting to compare the behavior of the cracks in Figs. 8 and 9. The early behavior appears to be fairly similar as the cracks develop into the microstructure surrounding the respective pores. Growth rates are seen to initially fluctuate between 10^{-6} and 10^{-5} mm/cycle for both cracks. When using a 3-pt sliding polynomial curve fit for data taken every 500 cycles, it is

seen that Crack D in Fig. 9 experienced more periods of arrest during initial crack growth than Crack A. These periods of arrest, where the surface crack length did not change over at least 1,500 cycles, are represented in Fig. 9 (b) with growth rate of 10^{-7} mm/cycle. While there is clear evidence from replication that both of these cracks had initiated within the first 50 cycles of loading, the scatter in the early crack growth behavior results in a greater than 2X difference in the final life of these specimens (N_f = 10,469 cycles for Specimen A and N_f = 23,458 for Specimen D). Quite notably, the transition crack size, beyond which the growth is seen to progress without deceleration or arrest, differs for these two cracks. Crack A in Fig. 8 grows continuously after surpassing a crack size of 93 μm (ΔK = 9.6 MPa-$m^{1/2}$), while Crack D in Fig. 9 continues to show significant fluctuations in growth behavior until it exceeds a size of 128 μm (ΔK = 11.2 MPa-$m^{1/2}$). While the local microstructure at the crack front is likely continuing to play a role at these sizes, it is suspected that the character of the initiating pore influenced the early crack growth behavior and the observed size at which the cracks transitioned to continuous growth. Based strictly on the 2-dimensional projection apparent from the fracture surfaces, the pore in Fig. 9 is smaller, with a diameter of about 33 μm, and more symmetrical than the pore in Fig. 8. The pore in Fig. 8 reaches a greater depth into the specimen (~50 μm) and has a higher aspect ratio, with a major diameter of about 70 μm. These differences will result in higher local stresses around the initiation site leading to a somewhat higher crack driving force for the crack in Fig. 8.

Ultimately, the fluctuations in crack growth rate reflect the competition between crack driving force and microstructural barriers to propagation. At elevated temperatures the crack driving force includes both cyclic and time-dependent contributions and therefore depends on factors such as the applied stress, temperature, frequency (and dwell time), environment, and the local stress state around the initiation site. While the applied stress, temperature, frequency, and environment were nominally equivalent for all of the cracks shown in Fig. 7, the local stress state at the initiation sites was variable. Additionally, despite the very equiaxed and fine grain structure in this alloy, the random nature of the microstructural barriers to propagation will contribute to the significant variability seen in early crack growth and apparently can play a substantial role up to sizes where the crack front is encountering as many as 50 to 70 grains. While the random grain orientation will result in local variations in resistance to plastic deformation ahead of the crack, it is also known that the properties of the grain boundaries will vary, which can present variations in the resistance to the time-dependent environmental mechanism of crack growth. Gao et al. [25] examined the role of grain boundary engineering on the fatigue resistance of ME3 at elevated temperature. They showed that increasing the fraction of "special" grain boundaries (i.e., those having a particular misorientation and high degree of atomic matching) increased the long crack growth resistance in the near-threshold regime. The enhanced resistance to crack growth appears to be directly related to a reduction of grain boundaries susceptible to the mechanism of oxygen diffusion and grain boundary embrittlement, as they observed a significant reduction in intergranular growth for the grain boundary-engineered alloy in the near-threshold regime. It is likely that the random nature of the grain boundary character is responsible, at least in part, for the mixed mode of intergranular and transgranular growth observed in the early crack growth for the no dwell loading condition, as seen in Figs. 4, 8, and 9. It is interesting to note, however, that the transition past the microstructurally-small crack regime is observed to occur at sizes (2c ~ 90 to 130 μm) markedly less than the crack size where the transition to fully intergranular growth is observed (2c ~210 to 250 μm). Here it is useful to emphasize that two transitions in fracture morphology are noted in

this study. First is the regime of rough surface layer attributed to relatively longer exposure to environment, which correlated with the end of the period where crack growth was marked by significant fluctuations in growth rate. Second is the transition from a mixed transgranular/intergranular crack growth to a purely intergranular mode, which did not appear to correspond to any alteration in the crack growth behavior. While the growth rate in the first regime is considered dominated by microstructural barriers, the second transition could be driven by mechanical factors such as plastic or process zone size relative to the microstructure, as stated previously. This might explain the persistence of mixed-mode fracture morphology beyond the initial transition.

3.2.3 Role of Initiating Feature

Under the loading conditions examined in this paper, we have observed that crack initiation in this alloy occurs from either pores or non-metallic particles (NMPs). The size distribution of these features has been reported in detail previously [4], and the equivalent diameter of initiating pores is typically about 30 μm and that of initiating NMPs is somewhat larger at about 60 to 100 μm. While the pores are smaller than the NMPs, they are also far more prevalent in the microstructure and more commonly observed as surface initiation sites. Further, it has been observed that cracks initiating from NMPs located at the specimen surface dominate the life-limiting, or worst-case, failures observed in this alloy under these testing conditions [2, 4].

As seen in Fig. 7, one of the naturally-initiated small cracks that was monitored with replication originated from a NMP, and this crack reached a critical size causing failure in less cycles than any of the other cracks initiating from pores. In fact, the total fatigue life for the specimen failing from the NMP (3,666 cycles) was almost 3 times shorter than that for Specimen A (10,469 cycles), which was the lowest life of the pore-initiated failures. Fig. 10 shows the fracture surface for the crack emanating from this NMP. The NMP is an oxide, which is glassy in appearance. Oxides are commonly found in powder-processed superalloys. Similar to the small cracks initiated from pores, the fracture surface in Fig. 10 shows a transition to fully intergranular growth at a crack length of about 230 μm and depth of about 110 μm. However, unlike the pore-initiated small cracks, which showed a mixture of transgranular and intergranular growth for cracks below this size, the early growth in Fig. 10 shows a higher predominance of transgranular growth. This is consistent with our observations of all other NMP-initiated surface cracks tested under these conditions. The reason for this higher preference for transgranular growth mode, when compared to cracks from pores, is not fully understood. It seems that the mechanism of stress-assisted environmental attack of grain boundaries is essentially inactive for the early crack growth away from the NMP. It is known that such NMPs are surrounded by a tensile residual stress field, owing to the elastic incompatibility and mismatch in thermal expansion properties between the γ matrix and the ceramic particle [28 - 30]. However, this leads to a higher local tensile stress and higher mean stress in the vicinity of the NMP during fatigue cycling, both of which would be thought to contribute to enhanced susceptibility to environmentally-assisted growth along grain boundaries and more intergranular growth. It is possible that the chemical composition of the γ matrix surrounding the NMP has been altered due to the presence of the particle, changing the local properties and influencing the preferred crack growth mode, but this has not been examined. It is also possible that the multiaxial stress state

ahead of a NMP, which will be different from that ahead of a pore due to the mismatch in mechanical properties, could reduce the propensity for oxygen diffusion along grain boundaries.

Fig. 11 compares the growth rate for the crack initiated from the NMP in Fig. 10 to the two cracks initiating from pores in Specimens A and D and previously discussed in Figs. 8 and 9, respectively. Similar to the data given in Figs. 8 and 9, growth rates were determined using a 3-pt sliding polynomial fit using surface length measurements taken every 500 cycles. It is seen that the growth rates for the NMP-initiated crack are comparable with that of the two cracks from pores for ΔK levels greater than about 11.3 MPa-$m^{1/2}$ (i.e., surface lengths, 2c, of about 130 μm and greater). However, for ΔK levels less than this, the crack from the NMP is seen to grow significantly faster than the cracks from the pores. Quite notably, the significant fluctuations in growth rates observed in the microstructurally-small crack regime for the pore-initiated cracks are not observed for the NMP-initiated crack. In other words, the crack initiated from the NMP shows no appreciable periods of deceleration or temporary arrest, like those seen for all of the pore-initiated cracks in Fig. 7. It is believed that the faster growth of this crack is due primarily to the tensile residual stress state surrounding the NMP.

3.2.4 Effect of Dwell

The introduction of a dwell period at peak load is known to influence the fatigue crack growth behavior of superalloys at elevated temperatures. Most studies have examined long crack growth behavior and report generally faster growth rates under dwell conditions due to the enhanced time-dependent contributions to crack growth, particularly oxidation-induced intergranular cracking [10 - 13, 31]. As discussed earlier in this paper, it is also commonly reported that the long crack threshold is often observed to increase with the application of dwell times. Fewer studies have looked in detail at small crack growth behavior under dwell loading conditions [2, 8, 14, 32]. The authors of the current paper have previously reported [2] that the application of 6 second dwell time at 650°C results in significantly faster small crack growth rates in IN100, where the results are shown in Fig. 2. The effect of dwell on the behavior of small cracks in this alloy is examined in more detail here.

The growth of naturally-initiated small cracks was monitored using a standard replication technique for specimens tested with 6 second dwell. Fig. 12 shows the crack length as a function of cycles for the small cracks measured under these conditions (650°C, 0.33 Hz, R = 0.05, σ_{max} = 1,150 MPa, 6 second dwell at peak load). The five small cracks represented for the dwell condition all initiated from pores and were monitored in two separate specimens (three cracks were measured in one specimen and two cracks were measured in a second specimen). With the application of the dwell period, many crack initiation sites were observed within single specimens. Only the most dominant cracks are included in Figs. 2 and 12. For comparison, Fig. 12 includes the length measurements for the small crack that initiated from a NMP under no-dwell loading and shown previously in Fig. 7. It is seen in Fig. 12 that the cracks tested with 6 second dwell grew much faster than the NMP-initiated crack tested with no dwell. This is also apparent in Fig. 2, where growth rates for cracks tested with 6 second dwell are seen to be over an order of magnitude faster than crack growth with no dwell at low ΔK levels.

An important observation from Figs. 2 and 12, is that the scatter in small crack growth behavior with 6 second dwell is significantly less than that observed for no dwell. In particular, the large fluctuations seen in the microstructurally-small crack regime for no dwell loading,

resulting from decelerations and temporary crack arrest, are not observed when the 6 second dwell period is applied. The lack of significant periods of crack deceleration or arrest under the dwell loading is due to the enhanced crack driving force resulting from the contributions of time-dependent mechanisms. Fig. 3 (c and d) show the influence of 0 and 6 second dwell time respectively on crack growth morphology, where it is clear that the growth mode is fully intergranular from the initial crack sizes at a dwell time of 6 seconds. Fig. 13 provides an example of crack growth morphology under 120 second dwell time, and the growth is also fully intergranular, but now shows more evidence of cavitation and more oxidation products on the fracture surface. The images in Fig. 3 (c and d) and Fig. 13 strongly suggest that the mechanism of stress-assisted oxidation along grain boundaries is dominant under the dwell conditions, and this driving force for crack growth overwhelms the microstructural barriers such that significant fluctuations in growth rate are not observed.

It was noted in the previous section that the initial ($2c < 230$ μm) crack growth mode for small cracks initiating from NMPs and tested without dwell is predominantly transgranular. Fig. 14 shows the fracture surface for a small crack initiated from a NMP and tested under 6 second dwell loading (650°C, 0.33 Hz, R = 0.05, σ_{max} = 1,100 MPa). The small crack growth mode is seen to shift to fully intergranular with the application of 6 second dwell. Therefore, while the initiating feature (NMP or pore) is seen to influence the early crack growth mode under loading with no dwell, the time dependent mechanism of environmentally-driven embrittlement of grain boundaries dominates under 6 second dwell loading, regardless of the crack initiating feature.

Table 1
Summary of crack growth morphology observed from fractography.

Initiation Site	Loading Condition	Crack Morphology a < ~120 μm	Crack Morphology a > ~120 μm
Surface Pore	No Dwell	TG / IG Mix	IG
Surface Pore	6 sec. Dwell	IG	IG
Surface NMP	No Dwell	TG	IG
Surface NMP	6 sec. Dwell	IG	IG
Sub-surface NMP	No Dwell	TG	TG
Sub-surface NMP	6 sec. Dwell	TG	TG

* *TG = Transgranular and IG = Intergranular*

Based on the fractographic observations highlighted in this paper, the general crack growth mode in this alloy is summarized in Table 1. It is noted that under the given loading conditions, three types of crack initiation sites were observed: pore located at the specimen surface, NMP located at the specimen surface, and NMP located in the specimen interior [2, 4]. No significant transition in crack growth mode is seen for subsurface growth, where regardless of dwell period

the crack growth is always transgranular. Similarly for surface initiated cracks grown under 6 second dwell, there is no transition in crack growth mode observed. Intergranular growth is always observed with this dwell time, regardless of whether the crack initiates from a pore or NMP. For a surface crack tested with no dwell, a transition to fully intergranular crack growth is observed for crack depths greater than about 120 μm. For sizes less than this depth, crack growth mode is seen to be a mixture of intergranular and transgranular. In addition, it is noteworthy that the initial growth from surface NMPs ($a < \sim 120$ μm) shows more predominance of transgranular growth than for cracks from surface pores. The reason for this is not fully understood.

4. Conclusions

Based on a systematic study of the long and small crack growth behavior in IN100 tested at 650°C, both with and without a 6 second dwell at peak loads, the following conclusions can be made:

1. The great majority of variability in fatigue life comes from crack initiation and early crack growth, where crack sizes are less than about 100 μm.

2. The life-limiting fatigue failures observed in this alloy are dominated by crack growth, where the crack initiation period can be assumed to be negligible.

3. A significant small crack effect is apparent in this alloy, where small cracks are observed to grow at ΔK levels less than the long crack thresholds and at faster rates than long cracks for a given ΔK. Additionally, long crack data can show a profoundly different response to loading variables such as dwell time.
    - While the 6 second dwell period showed essentially no effect on long crack growth rates (with the exception of a slight increase in ΔK_{th}), initial small crack growth rates were observed to be over an order of magnitude faster when tested with this dwell period.

4. The crack growth mode, as characterized from fracture surface morphology, is dependent upon loading condition (e.g., stress, frequency, environment), but does not provide a definitive indication of growth rate.
    - Intergranular crack growth requires that the crack tip be exposed to the environment. This mode of crack growth is believed to be dominated by a mechanism of stress-assisted diffusion of oxygen along grain boundaries resulting in the brittle fracture.

5. This alloy demonstrates two transitions in the growth behavior of small surface cracks tested under loading with no dwell (650°C, 0.33 Hz, R = 0.05, σ_{max} = 1,150 MPa).
    - The first transition appears to mark the passage beyond the microstructurally-small crack regime where significant fluctuations in early growth rates are observed, resulting from rapid growth followed by periods of deceleration and temporary arrest. The crack size at which this transition occurs was observed to

vary for cracks initiating from pores (2c ~ 90 to 130 μm) and depends on the local microstructure, as well as the character of the initiating pore (e.g., size, shape, orientation). Cracks initiating from NMPs do not show significant fluctuations in early growth rates, likely due to the enhanced crack driving force resulting from the tensile residual stress state in the surrounding γ matrix.

- The second transition is observed from fracture surface morphology, where a shift from mixed transgranular and intergranular growth mode to fully intergranular growth is evident. The size at which this transition occurs (2c ~210 to 250 μm) is seen to be quite repeatable from specimen to specimen, showing little dependence on the characteristics of the initiation site. It is thought to be driven by mechanical factors, such as the development of a critical plastic zone size or crack tip opening displacement.

6. Under 6 second dwell loading, these transitions in small crack growth behavior are not observed. The crack growth mode is always fully intergranular under this loading condition, and no significant fluctuations in early crack growth rates due to temporary deceleration and arrest are observed.

Acknowledgements

This work was performed at the Air Force Research Laboratory, Materials and Manufacturing Directorate, Wright-Patterson Air Force Base, OH. The partial financial support of the Defense Advanced Research Project Agency (DARPA) under DARPA orders M978, Q588, P699, and S271 with Dr. Leo Christodoulou as the program manager is gratefully acknowledged. Essential support was also provided by the Air Force Office of Scientific Research (AFOSR) with Dr. Victor Giurgiutiu as the program manager. The authors also wish to acknowledge Dr. Reji John, Dr. Jim Larsen, Dr. Chris Szczepanski, and Dr. Kezhong Li for their helpful technical discussions, Mr. Dale Osborne for his performance of the long crack testing, and Mr. Phil Buskohl and Mr. Eric Burba for their assistance with the replication-based small crack growth experiments.

References

[1] J. N. Yang and W. J. Trapp, *AIAA Journal*, Vol. 12, pp. 1623-1630, 1974.

[2] S. K. Jha, M. J. Caton, and J. M. Larsen, "Mean vs. life-limiting fatigue behavior of a nickel-based superalloy," Superalloys 2008, TMS, pp. 565-572, 2008.

[3] S. K. Jha, M. J. Caton, and J. M. Larsen, "A new paradigm of fatigue variability behavior and implications for life prediction," Materials Science and Engineering, **468-470**, pp. 23-32, 2008.

[4] S. K. Jha, M. J. Caton, and J. M. Larsen, " The mean vs. life-limiting fatigue response of a Ni-base superalloy, Part II: life-prediction methodology," Accepted in Metallurgical and Materials Transactions A, 2009.

[5] T. P. Gabb, J. Telesman, P. T. Kantzos, P. J. Bonacuse, and R. L. Barrie, NASA/TM-2002 211571, 2002.

[6] T. P. Gabb, P. J. Bonacuse, L. J. Ghosn, J. W. Sweeny, A. Chatterjee, and K. A. Green, NASA/TM-2000-209418, 2000.

[7] M. J. Caton, S. K. Jha, A. H. Rosenberger, and J. M. Larsen, "Divergence of mechanisms and the effect on the fatigue life variability of Rene`88DT," Superalloys 2004, TMS, pp. 305-312, 2004.

[8] H. T. Pang and P. A. S. Reed, "Fatigue crack initiation and short crack growth in nickel-base turbine disc alloys – the effects of microstructure and operating parameters," International Journal of Fatigue, **25**, pp. 1089-1099, 2003.

[9] I. S. Raju and J. C. Newman, Jr., "Stress intensity factors for circumferential surface cracks in pipes and rods under tension and bending loads," Fracture Mechanics: 17th Volume, ASTM STP 905, ASTM, pp. 789-805, 1986.

[10] S. P. Lynch, T. C. Radtke, B. J. Wicks, and R. T. Byrnes, "Fatigue crack growth in nickel-based superalloys at 500-700°C. I: Waspaloy," *Fatigue Fract. Engng. Mater. Struct.*, Vol. 17, No. 3, pp. 297-311, 1994.

[11] S. P. Lynch, T. C. Radtke, B. J. Wicks, and R. T. Byrnes, "Fatigue crack growth in nickel-based superalloys at 500-700°C. II: Direct-aged alloy 718," *Fatigue Fract. Engng. Mater. Struct.*, Vol. 17, No. 3, pp. 313-325, 1994.

[12] K. Sadananda and P. Shahinian, "Hold-time effects on high temperature fatigue crack growth in Udimet 700," *Journal of Materials Science*, Vol. 13, pp. 2347-2357, 1978.

[13] N. J. Hide, M. B. Henderson, and P. A. S. Reed, "Effects of grain and precipitate size variation on creep-fatigue behaviour of Udimet 720Li in both air and vacuum," Superalloys 2000, TMS, pp. 495-503, 2000.

[14] G. Onofrio, G. A. Osinkolu, and M. Marchionni, "Fatigue crack growth of Udimet 720 Li superalloy at elevated temperature," International Journal of Fatigue, **23**, pp. 887-895, 2001.

[15] J. Gayda and R. V. Miner, "The effect of microstructure on 650°C fatigue crack growth in P/M Astroloy," *Met. Trans. A*, Vol. 14A, pp. 2301-2308, 1983.

[16] H. H. Smith and D. J. Michel, "Effect of environment on fatigue crack propagation behavior of alloy 718 at elevated temperatures," Metallurgical and Materials Transactions A, **17A**, pp. 370-374, 1986.

[17] R. R. Stephens, L. Grabowski, and D. W. Hoeppner, "The effect of temperature on the behavior of short fatigue cracks in Waspaloy using an in situ SEM fatigue apparatus," *Int. J. Fatigue*, Vol. 15, pp. 273-282, 1993.

[18] M. Reger and L. Remy, "High temperature, low cycle fatigue of IN-100 superalloy II: influence of frequency and environment at high temperatures," Materials Science and Engineering A, **101**, pp. 55-63, 1988.

[19] J. C. Newman and I. S. Raju, "Stress-intensity factor equations for cracks in three-dimensional bodies subjected to tension and bending loads," in: Computational Methods in the Mechanics of Fracture, S. N. Atluri, Editor, Elsevier Science Publishers, pp. 312-334, 1986.

[20] J. P. Bentham and W. T. Koiter, Mechanics of Fracture 1: Method of analysis and solutions of crack problems, G. C. Sih, Editor, Noordhoff International Publishing Leyden, pp. 131-178, 1973.

[21] Y. Murakami et al., Stress intensity factors handbook vol. 2, Pergammon Press, Oxford, 1986.

[22] W. Carpenter, B. S. –J. Kang, and K. M. Chang, "SAGBO mechanism on high temperature cracking behavior," Superalloys 718, 625, 706 and Various Derivatives, TMS, pp. 679-688, 1997.

[23] U. Krupp, W. M. Kan, X. Liu, O. Dueber, C. Laird, and C. J., McMahon, Jr., "cracking behavior," Superalloys 718, 625, 706 and Various Derivatives, TMS, pp. 679-688, 1997.

[24] Z. Huang, C. Iwashita, I. Chou, and R. P. Wei, "Environmentally assisted, sustained-load crack growth in powder metallurgy nickel-based superalloys," Metallurgical and Materials Transactions A, **33A**, pp. 1681-1687, 2002.

[25] Y. Gao, M. Kumar, R. K. Nalla, and R. O. Ritchie, "High-cycle fatigue of nickel-based superalloy ME3 at ambient and elevated temperatures: role of grain-boundary engineering," *Metallurgical and Materials Transactions A*, **36A**, pp. 3325-3333, 2005.

[26] S. Suresh and R. O. Ritchie, "Propagation of short fatigue cracks," Int. Metals Rev., Vol. 29, pp. 445-476, 1984.

[27] J. Lankford, "The influence of microstructure on the growth of small fatigue cracks," *Fatigue Fract. Engng Mater. Struct.*, Vol. 8, pp. 161-175, 1985.

[28] D. A. Jablonski, "The effect of ceramic inclusions on the low cycle fatigue life of low carbon Astroloy subjected to hot isostatic pressing," *Materials Sci. Engng.*, Vol. 48, p. 189, 1981.

[29] M. M. Shenoy, R. S. Kumar, and D. L. McDowell, *Int J Fatigue*, Vol. 27, p. 113, 2005.

[30] R. Bullough and L. C. Davis, "The residual deformation fields in particle reinforced metal-matrix composites," *Acta Materialia*, Vol. 43, p. 2737, 1995.

[31] G. A. Osinkolu, G. Onofrio, and M. Marchionni, "Fatigue crack growth in polycrystalline IN 718 superalloy," *Materials Science and Engineering*, **A356**, pp. 425-433, 2003.

[32] F. Sansoz, B. Brethes, and A. Pineau, "Propagation of short fatigue cracks from notches in a Ni base superalloy: experiments and modelling," *Fatigue Fract Engng Mater Struct*, **25**, pp. 41-53, 2002.

Figures

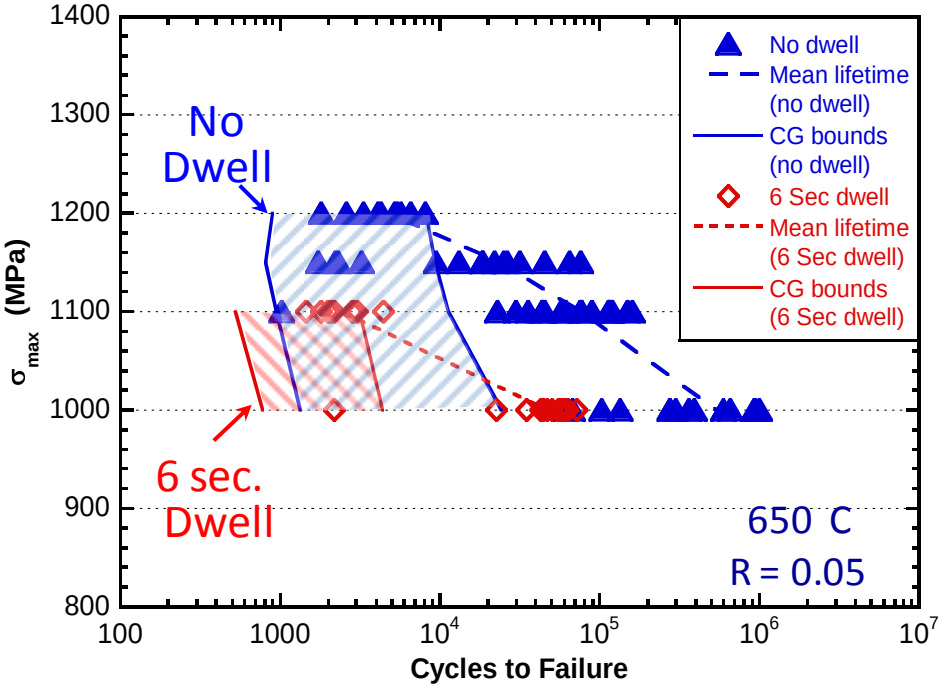

Fig. 1. Previously reported [2] fatigue lifetimes for IN100 tested at 650°C, 0.33 Hz, R = 0.05, and both with and without 6 second dwell at peak load. The hatched regions indicate the predicted range of fatigue crack growth life.

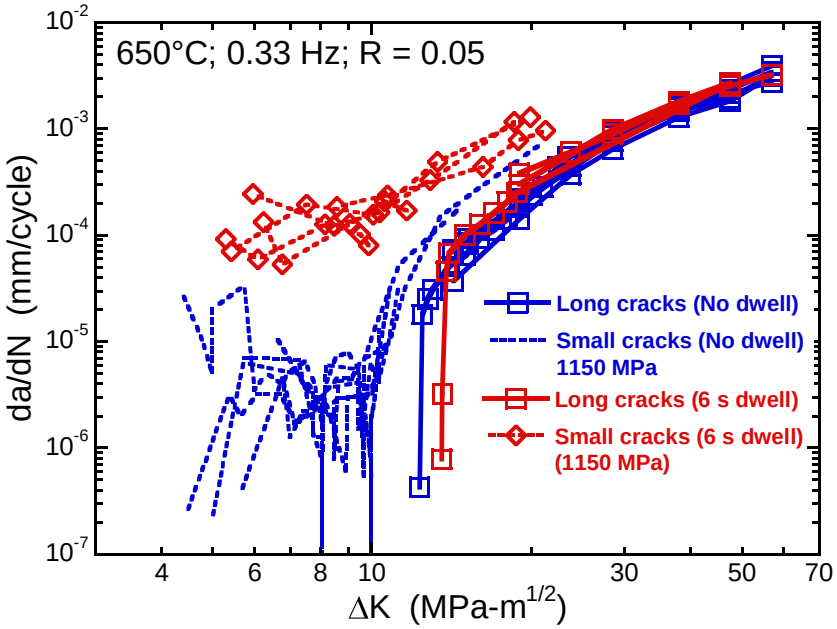

Fig. 2. Previously reported [2] long and small crack growth data for IN100 tested at 650°C, 0.33 Hz, R = 0.05 both with and without 6 second dwell loading.

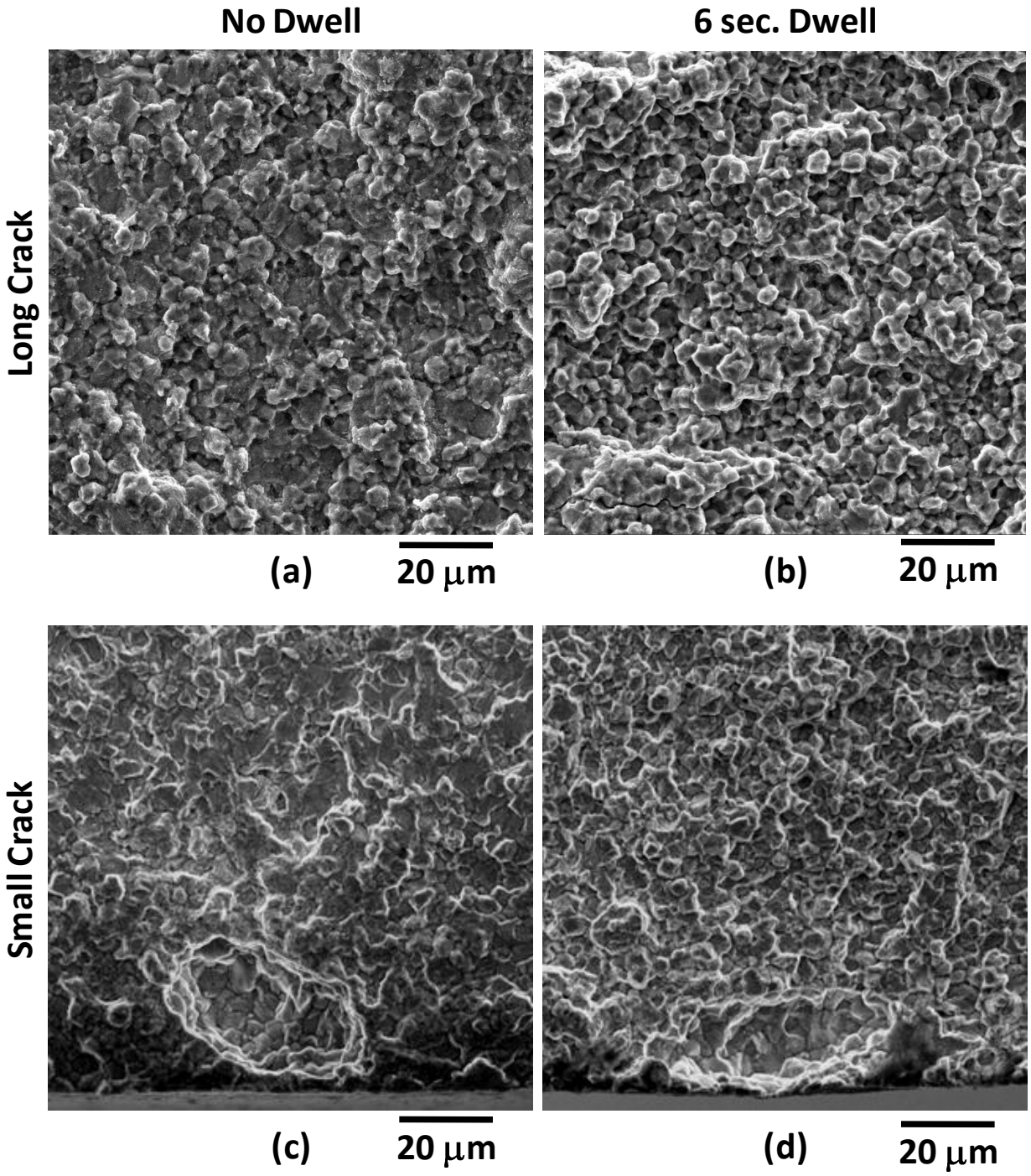

Fig. 3. (a) Fracture surface of long crack tested with no dwell at ΔK = 14.25 MPa-$m^{1/2}$. (b) Fracture surface of long crack tested with 6 second dwell at ΔK = 14.25 MPa-$m^{1/2}$. (c) Fracture surface of small crack tested with no dwell. (d) Fracture surface of small crack tested with 6 second dwell.

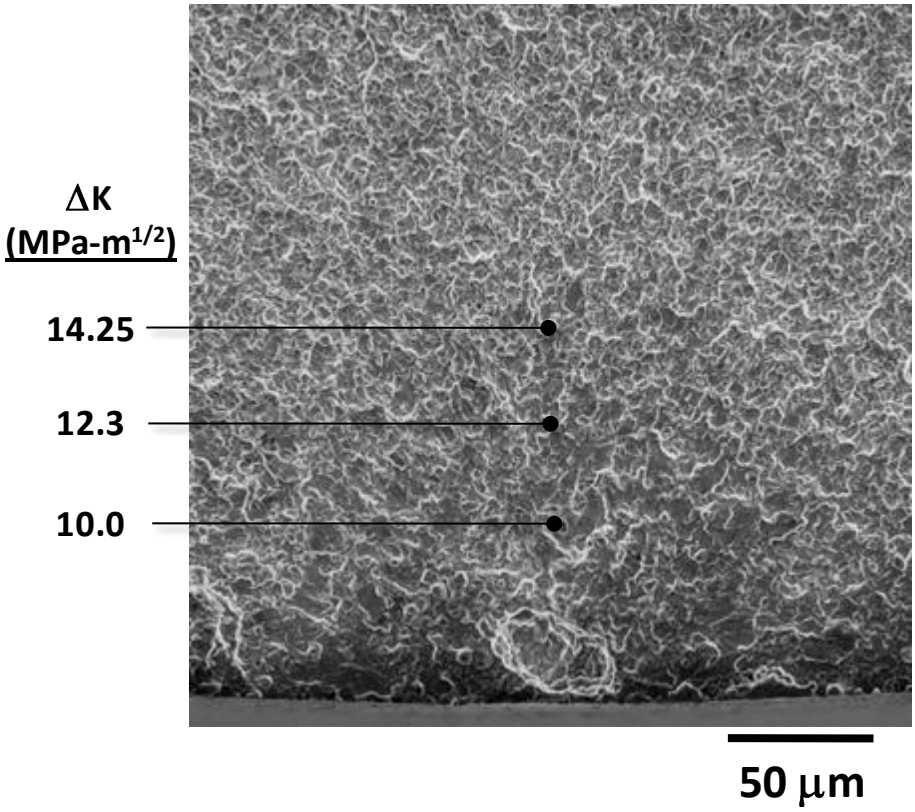

Fig. 4. Fracture surface of a small crack tested with no dwell showing a transition from mixed transgranular / intergranular growth to fully intergranular growth at a crack depth of ~ 135 μm ($\Delta K \sim 14.6$ MPa-$m^{1/2}$).

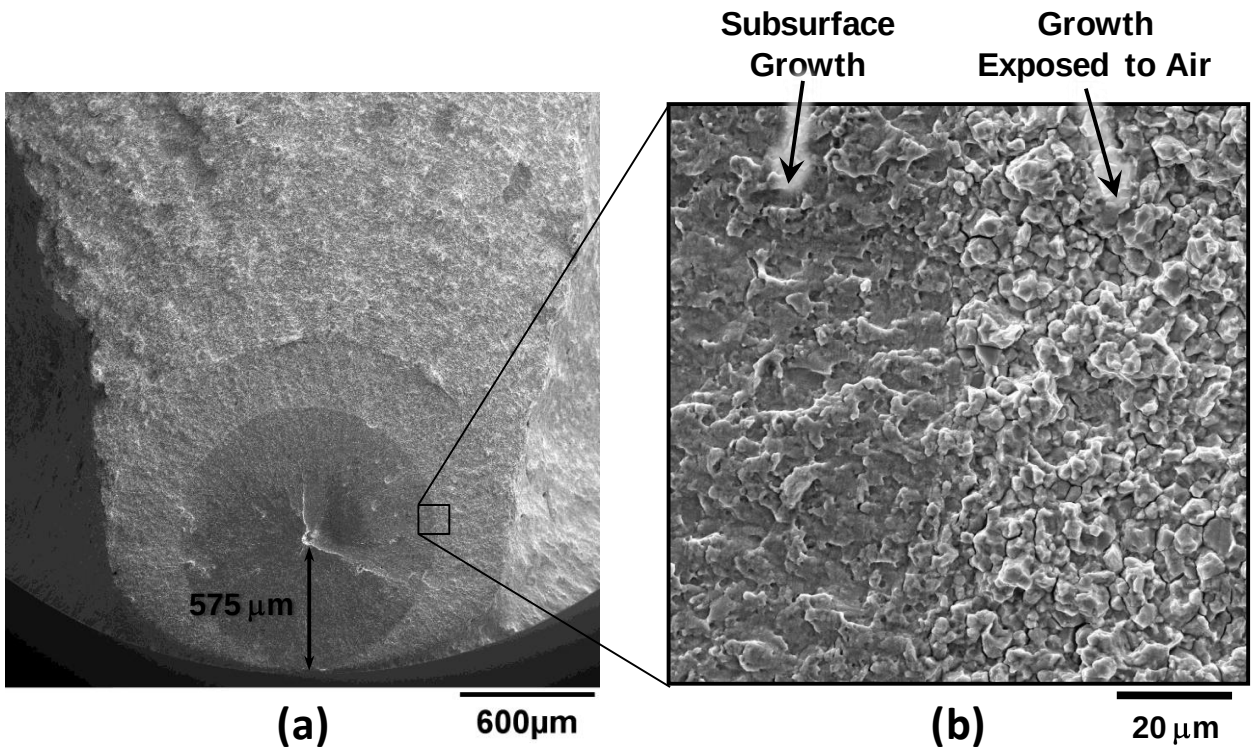

Fig. 5. (a) Fracture surface of a fatigue specimen tested with no dwell that failed from a subsurface crack initiation site (NMP). The test conditions for this specimen were 650°C, 0.33 Hz, R = 0.05, σ_{max} = 1,150 MPa, and no dwell. (b) High magnification image of the crack mode transition that occurs when the crack front is first exposed to environment.

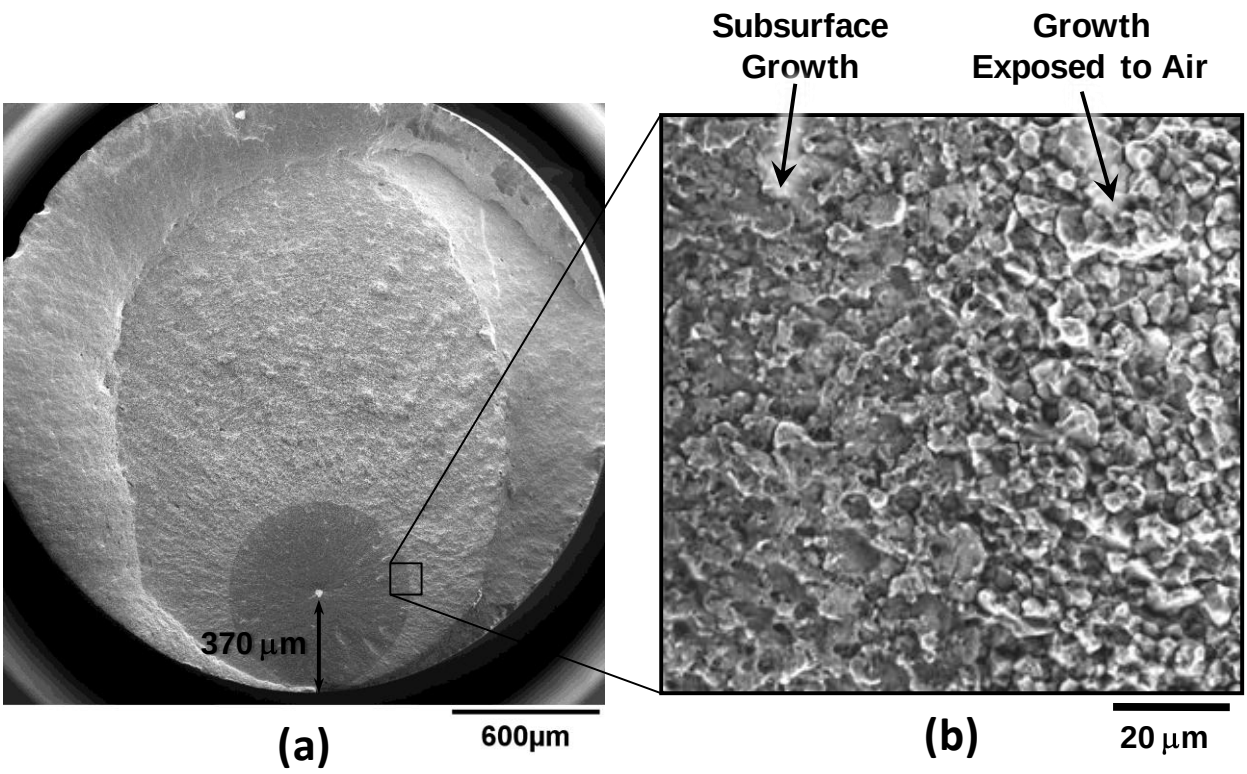

Fig. 6. (a) Fracture surface of a fatigue specimen tested with 6 second dwell that failed from a subsurface crack initiation site (NMP). The test conditions for this specimen were 650°C, 0.33 Hz, R = 0.05, σ_{max} = 1,000 MPa, and 6 sec. dwell. (b) High magnification image of the crack mode transition that occurs when the crack front is first exposed to environment.

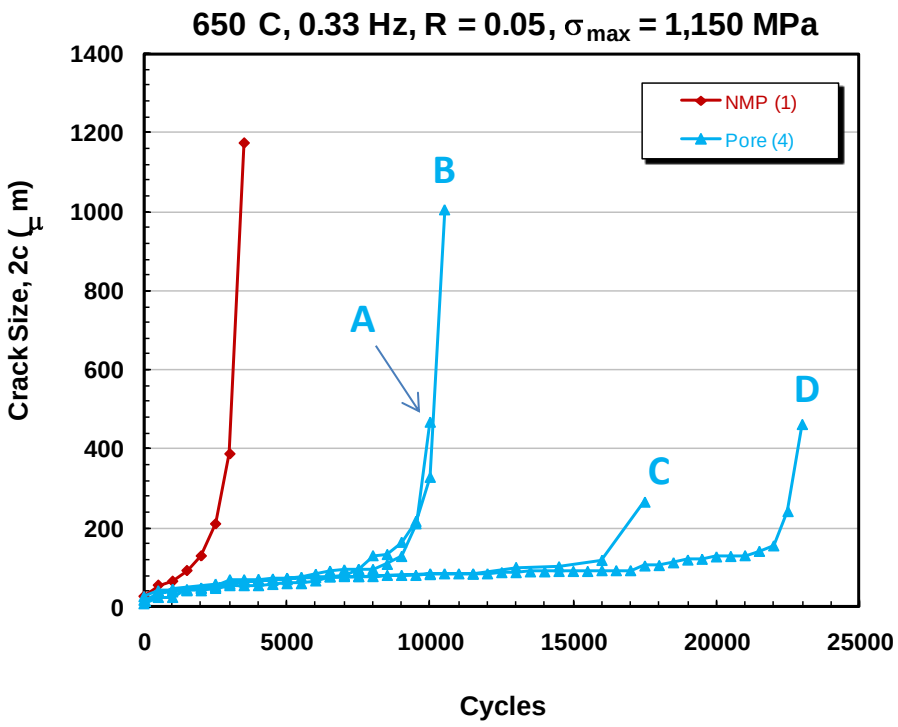

Fig. 7. Small crack length, 2c, measured from replication as a function of applied cycles for cracks in five separate specimens tested under the equivalent loading condition (650°C, 0.33 Hz, R = 0.05, σ_{max} = 1,150 MPa, No Dwell).

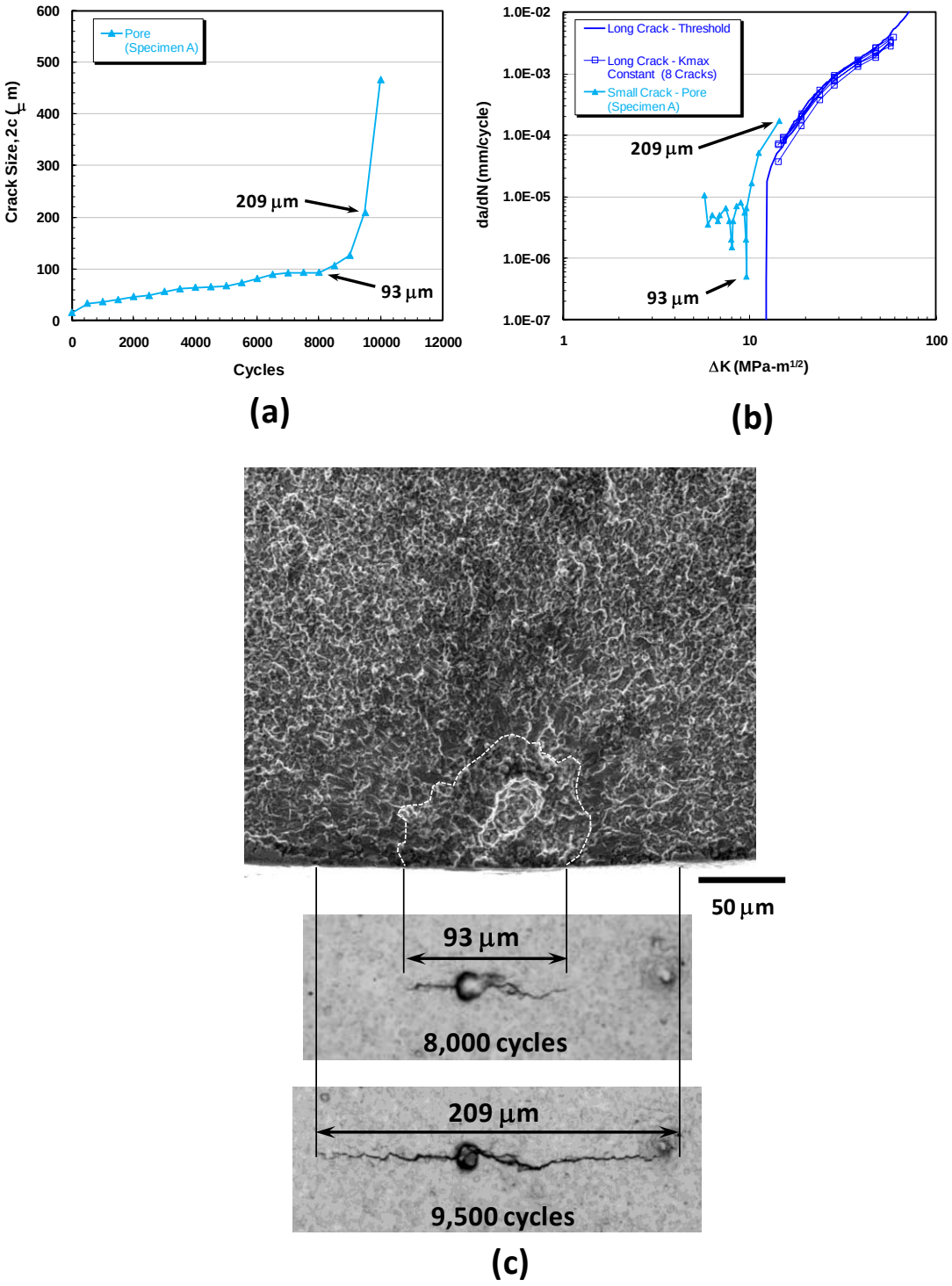

Fig. 8. (a) Crack length versus cycles for Specimen A from Fig. 7. (b) Crack growth rate as a function of ΔK for the crack in Specimen A. (c) Fracture surface for Specimen A and photos of two replicas showing the associated surface crack length at 8,000 and 9,500 cycles. The dashed white curve indicates the estimated crack shape at 2c = 93 μm, where the final significant period of temporary crack arrest was observed.

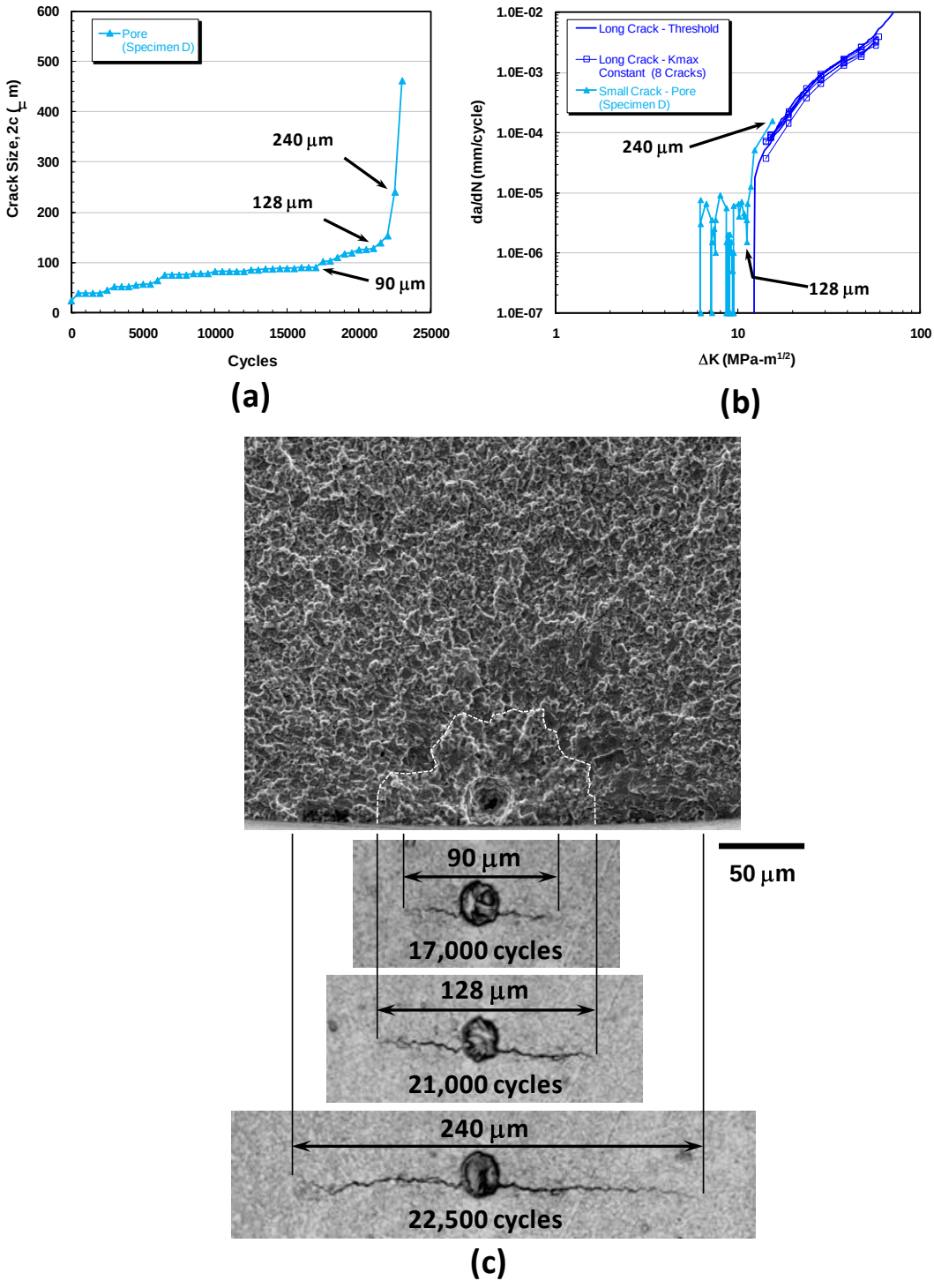

Fig. 9. (a) Crack length versus cycles for Specimen D from Fig. 7. (b) Crack growth rate as a function of ΔK for the crack in Specimen D. (c) Fracture surface for Specimen D and photos of three replicas showing the associated surface crack length at 17,000, 21,000, and 22,500 cycles. The dashed white curve indicates the estimated crack shape at 2c = 128 μm, where the final significant period of temporary crack arrest was observed.

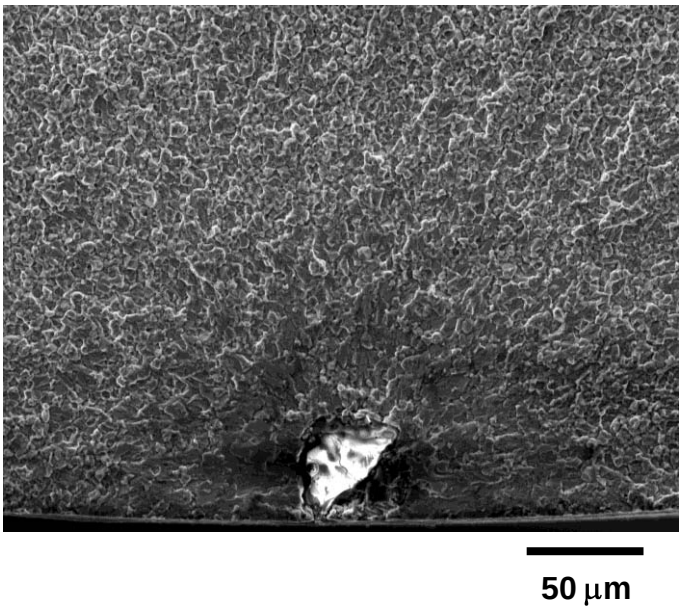

Fig. 10. Fracture surface for a small crack initiated from a NMP and tested at 650°C, 0.33 Hz, R = 0.05, σ_{max} = 1,150 MPa and with no dwell.

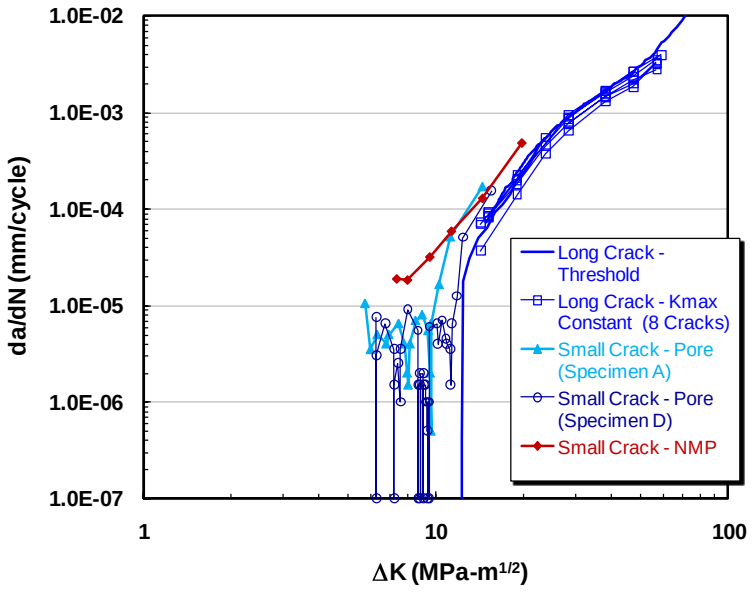

Fig. 11. Comparison of crack growth rates for small cracks initiating from a NMP and two pores tested at 650°C, 0.33 Hz, R = 0.05, σ_{max} = 1,150 MPa and with no dwell. Long crack data for the same loading conditions are included.

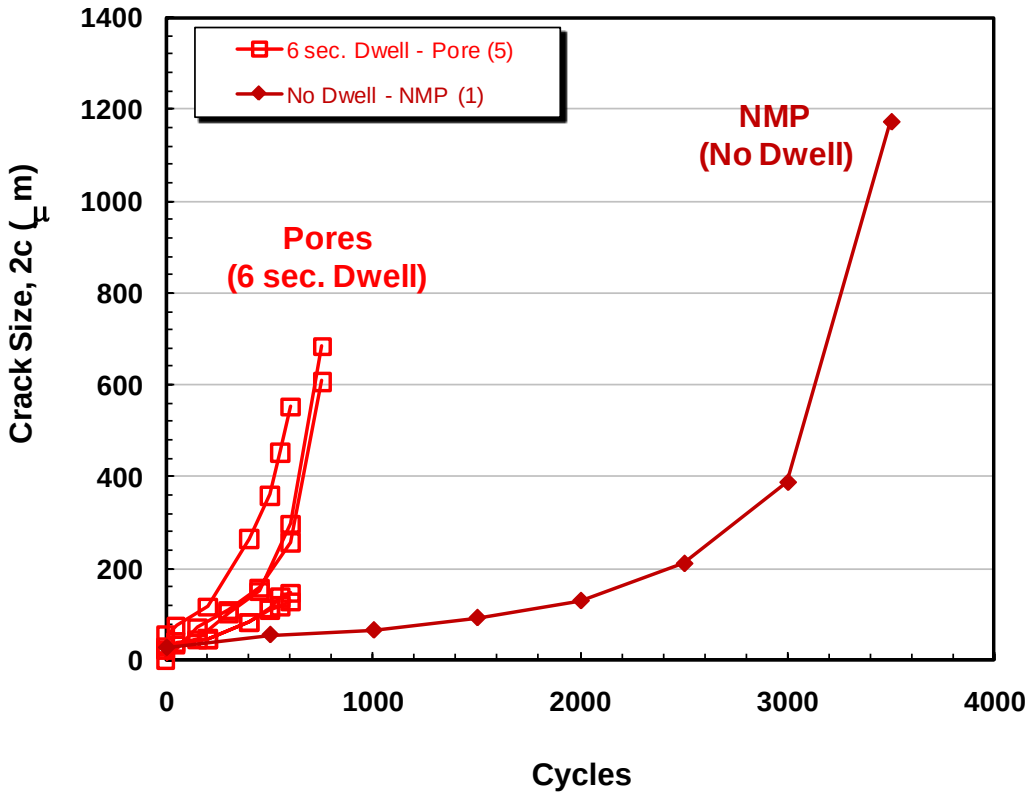

Fig. 12. Crack length as a function of cycles for five cracks initiated from surface pores and grown under 6 second dwell loading compared to a crack initiated from a NMP and tested with no dwell. All cracks were tested at 650°C, 0.33 Hz, R = 0.05, and σ_{max} = 1,150 MPa.

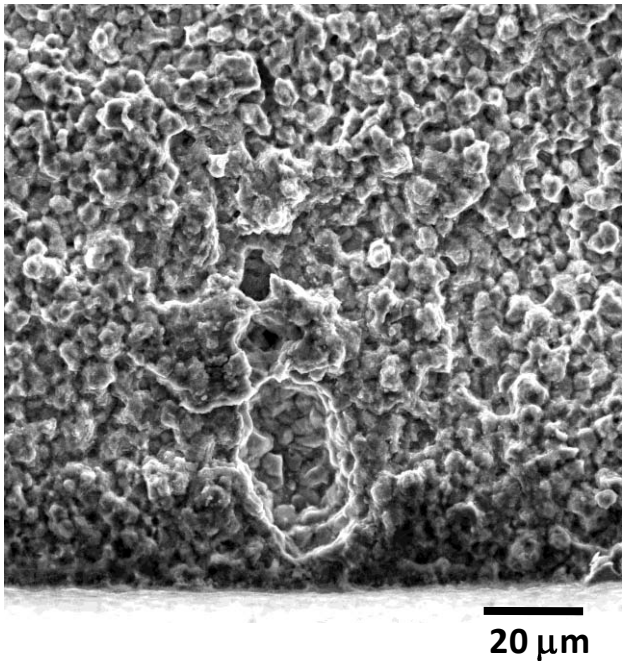

Fig. 13. Fracture surface showing small crack growth morphology for a crack initiating from a surface pore and tested at 650°C, 0.33 Hz, R = 0.05, σ_{max} = 1,000 MPa, and 120 sec dwell.

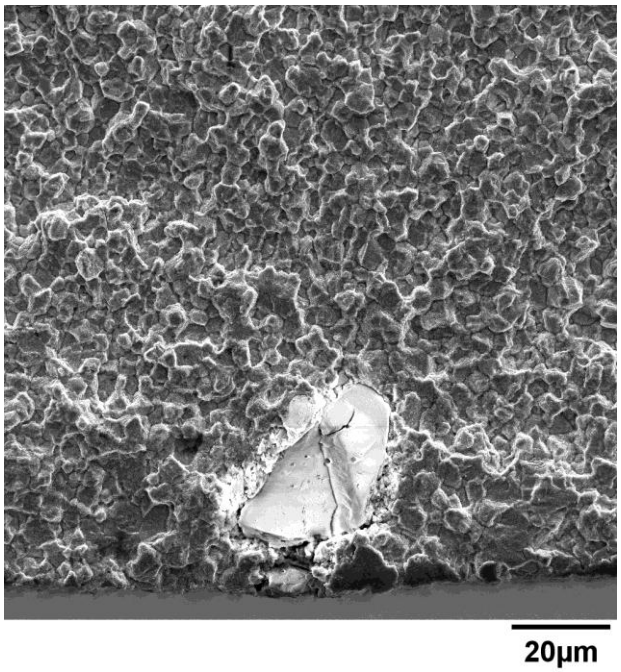

Fig. 14. Fracture surface showing small crack growth morphology for a crack initiating from a NMP and tested at 650°C, 0.33 Hz, R = 0.05, σ_{max} = 1,100 MPa with 6 second dwell.